A noval lightsheet scattering microscopy for long-term visualization of cell-ECM interaction

Xiangda Zhou [1], Renping Zhao [1], Archana K. Yanamandra [1,2], Carsten Kummerow [1], Markus Hoth [1], Bin Qu [1, 2]

[1] Biophysics, Center for Integrative Physiology and Molecular Medicine (CIPMM), School of Medicine, Saarland aUniversity, Homburg; [2] INM-Leibniz Institute for New Materials, Saarbrücken, Germany

Corresponding author:

Bin Qu

Biophysics
Center for Integrative Physiology and Molecular Medicine (CIPMM)
School of Medicine, Saarland University
66421 Homburg, Germany.

INM-Leibniz Institute for New Materials
66123 Saarbrücken, Germany.

Tel: +49 6841 16 16310
Fax: +49 6841 16 16302
Email: bin.qu@uks.eu

Abstract

Visualization cell interaction with the extracellular matrix (ECM) mesh works plays a central role in understanding cell behavior and the corresponding regulatory mechanisms by the environment *in vivo*. However, long term visualization of 3D matrix structures remains challenging mainly due to photobleaching or blind spot in the currently available approaches. In this paper, we developed a label-free method based on light-sheet microcopy, termed light-sheet scattering microscopy (LSSM), as a satisfactory solution to solve this problem. LSSM can reliably determine structure of collagen matrices from different origin including bovine, human and rat tail. We verified that the quality and intensity of collagen structure images acquired by LSSM did not decline with time. LSSM offers abundant wavelength choice for matrix structure, maximizing combination possibilities for fluorescence to label the cells. LSSM can be used for visualizing ECM-cell interaction in 3D for long term and characterization of cell-applied forces. Interestingly, we observed ultrathin thread-like structures between cells and matrix using LSSM, which was not to be seen by normal fluorescence microscopy. In summary, LSSM provides a robust approach to investigate the complex interplay between cells and ECM *in vitro* under *in vivo*-mimicking conditions.

Introduction

Under physiological conditions, immune cells and tumor cells encounter complex and dynamic three dimensional (3D) environments. To maintain 3D environments, extracellular matrix (ECM) composed of fibrous mesh networks serves as one main structural component. Concerning immune surveillance, interaction of ECM with immune cells and tumor cells plays an essential role in tuning the final outcome. Compelling evidence from in vitro and in vivo shows that there are channels/tunnels in ECM, which can be either created or expanded by immune cells, facilitating migration of the follower immune cells [1]. These channels could also contribute to metastasis of tumor cells [2]. When the channels in ECM are too narrow, the width serves as a speed limiting factor to restrain the migration of immune cells as well as the metastatic tumor cells (ref). To find their target cells in a timely manner, immune cells need to apply efficient searching strategies. Interestingly, different migration modes of immune cells have been reported, for example superdiffusive levy walk in brain [3] and subdiffusive persistent random walk in lymph nodes [4], which seem to differ in different target organs. Structural features of the ECM such as porosity and fiber alignment could shape the migration patterns, which is decisive for optimization of search efficiency of immune cells. Migration of cells in ECM per se results in structural changes in ECM [1, 5], cumulative effect of which could play an essential role in outcome of immune surveillance, especially under physiological or pathological conditions *in vivo*. To investigate this, long-term visualization of ECM-cell interaction with defined and controllable features in vitro will provide a powerful tool.

Long-term visualization of natural structure of ECM remains, however, technically very challenging. One of the most applied approaches is fluorescently labelling the matrix protein of interest [6]. However, due to photobleaching, this method does not offer a satisfactory solution for long-term visualization. There are numerous other approaches well established to image fibrillar collagen, such as electron microscopy and second hormonic generation microscopy [7, 8]. Although these methods enable visualization of matrix structure with a high resolution, they cannot be applied for live cell imaging. A recently emerged method confocal reflection microscopy utilizes reflection of light by the fibrous structure of the matrix [9], offering a possibility to visualize collagen structure without fluorescence, which can also be combined with live cell imaging for long term. However, with confocal reflection microscopy the subset of fibrous structures perpendicular to the imaging plane cannot be detected due to a blind spot, which results in incomplete information in 3D structure of the reconstructed networks [10].

In this paper, we developed a label-free method based on light-sheet microcopy, termed light-sheet scattering microscopy (LSSM) as a robust approach to visualize ECM structures without blind spot and photobleaching. LSSM is specially advantageous for imaging cell behavior in ECM mesh works for long term. Non-fluorescently labeled cells can be also visualized by LSSM. Notably, using LSSM we observed thin thread-like structure between cells and matrix, which was not to be seen by normal fluorescence microscopy. In addition, LSSM can be used to characterize forces exerted on matrix by the embedded cells.

Materials and methods

Reagents

Following reagents were used in this work: Atto Fluor 647 NHS-Ester (Succinimidylester), Atto Fluor 488 NHS-Ester (Succinimidylester), CellTrace CFSE Cell Proliferation Kit (ThermoFisher Scientific), and CellTrace Calcein Red-Orange AM (ThermoFisher Scientific). RatCol Rat Tail Collagen (4 mg/ml), FibriCol Type I Collagen Solution (bovine, 10 mg/ml) and VitroCol Type I Collagen Solution (Human, 3 mg/ml) were obtained from Advanced BioMatrix.

Cell preparation and cell culture

Human primary $CD4^+$ T cells were negatively isolated using CD4 T Cell Isolation Kit Human (Miltenyi) from peripheral blood mononuclear cells (PBMCs) of healthy donors [11]. $CD4^+$ T cells were stimulated with Dynabeads Human T-Activator CD3/CD28 (ThermoFisher Scientific) and cultured in AIM V Medium (ThermoFisher Scientific) with 10% FCS (ThermoFisher Scientific) at a density of 2×10^6 cells/ml. Human pancreatic beta cells 1.4E7 were purchased from Merck and cultured in RPMI-1640 medium (ThermoFisher Scientific) supplemented with 2 mM glutamine, 1% Penicillin-Streptomycin plus 10% FCS. SK-MEL-5 cells were cultured in MEM medium (ThermoFisher Scientific) containing 10% FCS and 1% penicillin-streptomycin. All cells were cultured at 37 °C with 5% CO_2.

Preparation of collagen matrices

Collagen solutions were prepared as previously described [12]. Briefly, chilled 10× PBS was added to collagen stock solution prior to neutralization with 0.1 M NaOH.

The neutralized collagen solution was further diluted to the desired concentrations with 1× PBS for structure visualization or with AIMV medium for live cell imaging. The collagen was then sucked into a glass capillary and kept at 37°C with 5% CO_2 for 40 min for polymerization.

Fluorescent labeling of collagen fibres

After polymerization, the collagen rod was pushed out of the capillary carefully and immersed in the freshly made Atto Fluor 647 NHS-Ester or Atto Fluor 488 NHS-Ester solution (50 μg/ml) for 10 min at room temperature, followed by three times washing with 1× PBS for 5min. For live cell imaging, additional steps were required as previously reported [6]. Briefly, the Atto Fluor 488 NHS-Ester stained collagen was brought back in acetic acid (20 mM) at 4ºC. Then mix the acid-dissolved fluorescently labeled collagen with non-labeled collagen in a ratio between 1:25-1:50. The cell pellet was resuspended in this mixed collagen solution and polymerization was conducted as describe above.

Imaging with light sheet microscopy

Imaging chamber was assembled according to the manufacturer's instructions. For LSSM, the combination of 445 nm laser (power 0.2 %), LBF 405/488/561/640, SBS LP 490-BP 420-470 with an exposure time of 30 ms was used if not mentioned otherwise. The samples were illuminated from single side if not mentioned otherwise. For fluorescence imaging modality, following settings were used: 561 nm laser (power 0.5 %), LBF 405/488/561/640, SBS LP 560-LP 585 with an exposure time of 100 ms for calcein red-orange; 488 nm laser (power 1.0 %), LBF 405/488/561/640, SBS LP

490-BP 505-545, with an exposure time of 30 ms was used for Atto 488; 638 nm laser, SBS LP 560-LP 660 was used for Atto 647; 488 nm laser (power 0.5 %), LBF 405/488/561/640, SBS LP 510-BP 525-565 with an exposure time of 80 ms for CFSE. Time lapse with Z-stacks was conducted with an 20× objective at 37ºC. The intervals and total length of visualization were elaborated in the corresponding figure legend.

For live cell imaging, the cells were loaded with calcein red-orange (50 μM) at 37°C for 30 min or with CFSE (50 μM) at room temperature for 15 min. CFSE-stained cells were recovered in the incubator for 24 hours prior to imaging. The cells were centrifuged and the pellet was resuspended in the collagen solution followed by 40 min-polymerization and 1 hour recovery in the incubator. 3D reconstruction, maximum intensity projection (MIP) and channel merge were generated with Software Zen Black Edition (Zeiss). Tracking of collagen matrix displacement was manually carried out with the ImageJ plugin MTrackJ as reported elsewhere [13]. Colocalization was analyzed using ImageJ plugin JACoP (Just Another Colocalization Plugin) [14].

Results

LSSM is a label-free robust method to visualize collage structure

In order to develop an approach to visualize cell-ECM interaction for long term, we sought for establishing a label-free method based on light-sheet microscopy, which illuminates samples using a sheet of light. Inspired by the principle of confocal reflection microscopy, we investigated whether similar images could be obtained by light-sheet microscopy. To this end, we prepared type I bovine collagen samples in glass capillaries and visualized the collagen sample with various lasers (405 nm, 445 nm, 488 nm, 515 nm, 561 nm, 638 nm) in combination with different block filters, beam splitters and detection filters as summarized in Supplementary Fig. 1A. The acquired images show that among 216 possible combinations, the collagen structure were seen in 35 combinations (Supplementary Fig. 1B), which share a common feature: the combination of the block filter, the beam splitter and the detection filter does not exclude the wavelength of the excitation laser. In comparison, many of these working combinations do exclude theoretical emission wavelength of the auto-fluorescence, which could be excited by the corresponding laser. Out findings indicate that the structure of matrices are visualized by the scattered light. This technique is thus termed light-sheet scattering microscopy (LSSM). Of note, during acquisition a very low laser power (0.2%) and short exposure time (150 ms) were applied, suggesting that photocytotoxicity induced by LSSM is very low if not negligible, and that a fast scan speed can be achieved.

To verify whether the matrix structure acquired by LSSM reflects the original structure

of the matrix, we fluorescently labeled human collagen and scanned the same samples using LSSM and fluorescence microscopy concurrently. The results show that the fibrous structures and reconstructed 3D structures visualized by LSSM and fluorescence microscopy are very similar (Fig. 1A). To examine the robustness of LSSM, we further analyzed the collagen from different origin such as bovine (Fig. 1B) and rat tail (Fig. 1C). The results show that LSSM reliably obtained the key structural features of collagen matrix with different concentration and pore size as verified with the results from the fluorescence microscopy (Fig. 1).

No blind spot and no photobleaching in LSSM

In confocal reflection microscopy, a blind spot has been reported, resulting in around half of the fibers, which are vertically oriented above 50 degrees from the focal plane, missing in image data acquired by confocal reflection imaging modality [15]. We then also explored whether LSSM had the same limitation. For LSSM we chose dual side fusion mode, in which the samples were illuminated from both the left and the right side sequentially and the images from both sides were merged to generate the final image (Fig. 2A). We noticed that although not many, a few fibers did appear in images from only one side (Fig. 2B, Scattering Mode, insets 1-2), indicating that in LSSM modality illumination from only one side could leave a few fibers undetected, presumably due to the orientation of the fibers. Interestingly, a few thin fibrous structures which were detected only in LSSM (Fig. 2B, Merge, inset 1), implying that for thin fibers LSSM could achieve a better resolution compared to fluorescence microscopy, especially for thin fibrous structures.

In addition, the fibrous structures obtained by LSSM dual side fusion and fluorescence microscopy overlapped to a large extend (Fig. 2B). We analyzed colocalization between images obtained by scattering modality and by fluorescence modality in 3D. One example is shown in Fig. 2C and Movie 1-3. Manders' coefficients (M1 scattering over fluorescence and M2 fluorescence over scattering) are 0.689±0.038 (M1) and 0.643±0.022 (M2) for bovine samples, 0.756±0.051 (M1) and 0.725±0.068 (M2) for human samples, 0.577±0.129 (M1) and 0.696±0.064 (M2) for rat tail samples, further confirming that LSSM can reliably visualize matrix structures. Of note, we noticed that for fluorescent labelling under suboptimal conditions, staining efficiency might vary with different depths in the samples (Fig. 2D, Fluorescence). In this case, the scattering modality could still visualize the complete structure (Fig. 2D, compare Scattering and Fluorescence), highlighting the advantages of LSSM over fluorescence labelling.

Photobleaching is the bottle neck for long-term visualization, at least for fluorescence microscopy. We next analyzed photobleaching in LSSM. Images of fluorescently labeled collagen matrices were acquired concurrently using LSSM and fluorescence imaging modality every 30 sec for 6 hours. Time lapse images and the analysis show a substantial photobleaching in fluorescence microscopy, while no photobleaching was detected in LSSM (Fig. 2E, F). This technical advantage of LSSM enables reliable long-term visualization of dynamic change of matrix structures as well as matrix-cell interaction.

Application of LSSM to investigate cell-ECM interaction

Characterization of ECM-cell interaction is essential to understand the behavior of cells

in 3D. We examined whether LSSM could be applied to meet this purpose. We first loaded SK-MEL-5 cells, a melanoma cell line, with calcein red-orange and embedded the cells in Atto 488 labeled collagen matrix. Z-stacks of the samples were taken at 37ºC every 30 sec for about half an hour. Interestingly, in LSSM, the SK-MEL-5 cells were also detected, which could be morphologically distinguished from the mesh network of collagen matrix (Fig. 3A). Unexpectedly, highly dynamic filamentous structures linking the cells and the mesh network were detected in LSSM, which were not fluorescent (Fig. 3A, Movie 4), implying that those structures are not originated from the collagen matrix but rather from the SK-MEL-5 cells. Time lapse images from LSSM show that these dynamic filamentous structures were formed between SK-MEL-5 cells and the matrix when the cells moved away from the matrix (Fig. 3A, 7.5 min and 8 min, Movie 4), and also formed between SK-MEL-5 cells when the two cells migrated apart (Fig. 3A, 20 min and 20.5 min, Movie 4).

To identify whether these filamentous structures are unique to SK-MEL-5 cells, we used 1.4E7 cells, a human pancreatic beta cell line. Again, highly dynamic ultrathin filamentous structures between the cells and the mesh network were observed in LSSM, which were not fluorescent (Fig. 3B inset, Movie 5 highlighted in the upper frame). In addition, distortion of the matrix caused by cell contraction was also observed in both imaging modalities (Movie 5, highlighted in the lower frame). 3D reconstructions and the depth map further reveal that those filamentous structures were parallelly orientated in 3D and could be traced back to the cell body (Fig. 3C). These findings indicate that these LSSM-identified filamentous structures could play an essential role in regulating

ECM-cell interaction and cell-cell interaction, especially in 3D environments.

We examined whether LSSM is suitable to visualize fast migrating immune cells and their interaction with ECM. We loaded primary human $CD4^+$ T cells with CFSE, and visualized T cell migration in label-free 3D collagen matrices using LSSM in combination with fluorescence microscopy. Channels in collagen matrices were detected in LRSM as reported before using fluorescence microscopy [1]. We observed that after entry into the channel, the T cell first chose the segment with a narrower width (Fig. 3D, highlighted by the white arrowhead, Movie 6), expanded the channel and then reversed the direction and advanced to the other segmentation (Fig. 3D, highlighted by the grey arrow head, Movie 6). That result shows that LSSM is a powerful tool to characterize migration behavior defined/influenced by matrix structures.

Mechanical forces have been revealed recently as an essential factor to modulate cell function and the interplay between ECM and cells. When cells exert mechanical forces on the matrix, deformation of matrix is induced and can be used to characterize the mechanical forces exerted by the cells [16, 17]. Using LSSM, this deformation could be observed as shown in Movie 5. We further examined whether this deformation could be characterized with LSSM for long-term measurements. To this end, we embedded non-fluorescently labeled SK-MEL-5 cells in collagen matrices and acquired images every 1 min for 2 hours. Time lapse images show that in LSSM imaging modality, SK-MEL-5 cells could be well distinguished based on the morphology, and collagen fibers between two SK-MEL-5 cells were reorientated and aligned towards the cells at macroscopic length scale (Fig. 3E, F, Movie 7). These results indicate that LSSM is a

valid alternative method to characterize cell-applied mechanical forces.

Discussion

LSSM utilizes the light scattered sidewards by the collagen fibers, which is detected by the objective perpendicular to the imaging plane. Here, the imaging plane is illuminated by a thin sheet of light, the incidence angle of which is parallel to the imaging plane. In comparison, images taken by confocal reflection microscopy are formed from the light reflected by the collagen fibers. Therefore, the fibers vertically orientated to the imaging plane are not detected, leading to an artefact that 3D reconstructed matrix structures seem to be aligned to the imaging plane. For LSSM, however, the possibility for a total reflection by a fiber leading to a blind spot is theoretically extremely low. As shown in our results, the fibrous structures oriented to all directions were observed, and no discontinuation of vertically oriented fibers in 3D reconstructed networks were detected. In addition, since LSSM uses the scattered light, the signal intensity is not reduced with time. Thus, LSSM is shown to be a reliable label-free method to visualize mesh networks without photobleaching, which is especially advantageous for long-term measurements.

One unique feature of LSSM is that this imaging modality can also detect cells with or without fluorescent labeling. Observation of microscopic interaction between cell plasma membrane and the matrix can be therefore partially interfered. However, fluorescently labeling cell plasma membrane can overcome this technical limitation to a large extent. In addition, this feature enables visualization of 3D migration of non-fluorescently labeled cells, which can be beneficial to investigate 3D behavior of the

cells with difficulties for fluorescence labeling.

In this work, one unexpected observation with LSSM is the ultrathin filamentous structures between diverging cells or between matrices and the leaving/departing cells. Since these structures were not detected in fluorescence microscopy and the collagen was fluorescently labelled, the ultrathin filamentous structures should be originated from the cells. This postulation is further supported by our observation of these structures generated between diverging cells. These ultrathin structures could be derived from plasma membrane with or without architectural support of cytoskeleton. These intracellular filamentous structures could mediate ECM-cell or cell-cell interaction or exert force even without direct physical contact. The origin, generation mechanism and functions of these newly discovered structures require further investigation.

Mechanical interplay between cells and matrix plays a pivotal role in cell migration, function, differentiation and self-organization [16-20]. Cell-cell distant mechanical communications via matrix is essential for cell self-assembly [17]. Traction forces generated by cells lead to matrix deformation, enabling force transmission to distant cells. In a 3D scenario, traction forces generated by a single cell or spheroid can be well determined by traction force microscopy, which measures the displacement of microbeads evenly distributed in the matrix [21, 22]. For cell-cell distant mechanical communication, where two distantly located cells simultaneously apply forces on matrix mesh network, the displacement of the beads per se might not be suitable to reflect the forces applied as in the case for tug-of-war. In this case, real-time

visualisation of matrix deformation using LSSM offers an approach to determine force generation and transmission. In this work, we observed that collagen fibers were aligned between two SK-MEL-5 cells. Emerging evidence shows that aligned matrix potentiates cell migration to a fast mode [19]. We propose that this cell-induced transient local alignment of matrix could be used by immune cells as directional cues to quickly find their target cells.

In summary, we present LSSM as a reliable and robust tool for long-term visualization of ECM-cell interaction, which can be used to address important scientific questions, for example cell-cell distant mechanical communications, long-range traction force transmission, and how dynamic ECM structures reshape immune cells migration patterns and so on.

Acknowledgements

We thank the Institute for Clinical Hemostaseology and Transfusion Medicine for providing donor blood; Carmen Hässig, Cora Hoxha, Sandra Janku, and Gertrud Schäfer for excellent technical help. This project was funded by the Deutsche Forschungsgemeinschaft (SFB 1027 Project A2 to BQ, and GZ: INST 256/419-1 FUGG to MH), and by Bundesministerium für Bildung und Forschung (031L0133 to MH). The authors declare no competing financial interests.

Ethical considerations

Research carried out for this study with healthy donor material (leukocyte reduction system chambers from human blood donors) is authorized by the local ethic committee (84/15; Prof. Dr. Rettig-Stürmer).

References

[1] Z. Sadjadi, R. Zhao, M. Hoth, B. Qu, H. Rieger, Migration of Cytotoxic T Lymphocytes in 3D Collagen Matrices, Biophys J 119(11) (2020) 2141-2152.

[2] E. Wagenblast, M. Soto, S. Gutierrez-Angel, C.A. Hartl, A.L. Gable, A.R. Maceli, N. Erard, A.M. Williams, S.Y. Kim, S. Dickopf, J.C. Harrell, A.D. Smith, C.M. Perou, J.E. Wilkinson, G.J. Hannon, S.R. Knott, A model of breast cancer heterogeneity reveals vascular mimicry as a driver of metastasis, Nature 520(7547) (2015) 358-62.

[3] T.H. Harris, E.J. Banigan, D.A. Christian, C. Konradt, E.D. Tait Wojno, K. Norose, E.H. Wilson, B. John, W. Weninger, A.D. Luster, A.J. Liu, C.A. Hunter, Generalized Levy walks and the role of chemokines in migration of effector CD8+ T cells, Nature 486(7404) (2012) 545-8.

[4] M.F. Krummel, F. Bartumeus, A. Gerard, T cell migration, search strategies and mechanisms, Nat Rev Immunol 16(3) (2016) 193-201.

[5] F.H. Barnett, M. Rosenfeld, M. Wood, W.B. Kiosses, Y. Usui, V. Marchetti, E. Aguilar, M. Friedlander, Macrophages form functional vascular mimicry channels in vivo, Sci Rep 6 (2016) 36659.

[6] A.D. Doyle, Fluorescent Labeling of Rat-tail Collagen for 3D Fluorescence Imaging, Bio Protoc 8(13) (2018).

[7] T. Starborg, N.S. Kalson, Y. Lu, A. Mironov, T.F. Cootes, D.F. Holmes, K.E. Kadler, Using transmission electron microscopy and 3View to determine collagen fibril size and three-dimensional organization, Nat Protoc 8(7) (2013) 1433-48.

[8] X. Chen, O. Nadiarynkh, S. Plotnikov, P.J. Campagnola, Second harmonic generation microscopy for quantitative analysis of collagen fibrillar structure, Nat Protoc 7(4) (2012) 654-69.

[9] A.O. Brightman, B.P. Rajwa, J.E. Sturgis, M.E. McCallister, J.P. Robinson, S.L. Voytik-Harbin, Time-lapse confocal reflection microscopy of collagen fibrillogenesis and extracellular matrix assembly in vitro, Biopolymers 54(3) (2000) 222-34.

[10] L.M. Jawerth, S. Munster, D.A. Vader, B. Fabry, D.A. Weitz, A blind spot in confocal reflection microscopy: the dependence of fiber brightness on fiber orientation in imaging biopolymer networks, Biophys J 98(3) (2010) L1-3.

[11] C. Kummerow, E.C. Schwarz, B. Bufe, F. Zufall, M. Hoth, B. Qu, A simple, economic, time-resolved killing assay, Eur J Immunol 44(6) (2014) 1870-2.

[12] R. Schoppmeyer, R. Zhao, M. Hoth, B. Qu, Light-sheet Microscopy for Three-dimensional Visualization of Human Immune Cells, J Vis Exp (136) (2018).

[13] E. Meijering, O. Dzyubachyk, I. Smal, Methods for cell and particle tracking, Methods Enzymol 504 (2012) 183-200.

[14] S. Bolte, F.P. Cordelieres, A guided tour into subcellular colocalization analysis in light microscopy, J Microsc 224(Pt 3) (2006) 213-32.

[15] J.C. Grew, J.L. Ricci, H. Alexander, Connective-tissue responses to defined biomaterial surfaces. II. Behavior of rat and mouse fibroblasts cultured on microgrooved substrates, J Biomed Mater Res A 85(2) (2008) 326-35.

[16] C.J. Underwood, L.T. Edgar, J.B. Hoying, J.A. Weiss, Cell-generated traction forces and the resulting matrix deformation modulate microvascular alignment and growth during angiogenesis, Am J Physiol Heart Circ Physiol 307(2) (2014) H152-64.

[17] C.D. Davidson, W.Y. Wang, I. Zaimi, D.K.P. Jayco, B.M. Baker, Cell force-mediated matrix reorganization underlies multicellular network assembly, Sci Rep 9(1) (2019) 12.

[18] J. Francois, A. Kandasamy, Y.T. Yeh, A. Schwartz, C. Ayala, R. Meili, S. Chien, J.C. Lasheras, J.C. Del Alamo, The interplay between matrix deformation and the coordination of turning events governs directed neutrophil migration in 3D matrices, Sci Adv 7(29) (2021).
[19] W.Y. Wang, C.D. Davidson, D. Lin, B.M. Baker, Actomyosin contractility-dependent matrix stretch and recoil induces rapid cell migration, Nat Commun 10(1) (2019) 1186.
[20] S.B. Han, J.K. Kim, G. Lee, D.H. Kim, Mechanical Properties of Materials for Stem Cell Differentiation, Adv Biosyst 4(11) (2020) e2000247.
[21] C. Franck, S.A. Maskarinec, D.A. Tirrell, G. Ravichandran, Three-dimensional traction force microscopy: a new tool for quantifying cell-matrix interactions, PLoS One 6(3) (2011) e17833.
[22] L. Hazlett, A.K. Landauer, M. Patel, H.A. Witt, J. Yang, J.S. Reichner, C. Franck, Epifluorescence-based three-dimensional traction force microscopy, Sci Rep 10(1) (2020) 16599.

Figure legends

Figure 1. Collagen structures visualized by LSSM reflect the natural mesh networks. Collagen from human (**A**, 2mg/ml), bovine (**B**, 2 and 4 mg/ml) or rat tail (**C**, mg/ml) was used. Collagen was fluorescently labeled with Atto 488. Z-stacks with step-size of 0.4 µm for 95 slices (**A**) or for 119 slices (**B** and **C**) were acquired. Scale bars are 40 µm. Representative images from at least three independent experiments are shown.

Figure 2. No blind spot and photobleaching in LSSM. (**A**) Sketch for single side illumination. (**B-D**) Comparison of images from LSSM and fluorescence microscopy. Rat tail collagen (2 mg/ml) was fluorescently labeled with Atto 488. Images from single side illumination (**B**) and the merged images of both sides (dual side fusion, **B-D**) are shown. Z-stacks with step-size of xx µm for xx slices were obtained with LSSM and fluorescence mode subsequentially at 37ºC. (**E**, **F**) Signal intensity obtained by LSSM is not reduced with time. Bovine collagen (2 mg/ml) was labeled with Atto 647. Z-stacks with step-size of 0.621 µm for 50 slices were obtained with LSSM and fluorescence mode subsequentially at 37ºC every 30 sec for 6 hours. Scale bars are 40 µm. Representative images from at least three independent experiments are shown.

Figure 3. Live cell imaging with LSSM. (**A-C**) Ultrathin filamentous structures observed with LSSM. Rat tail collagen (2 mg/ml) was fluorescently labeled with Atto 488. Calcein red-orange loaded SK-MEL-5 cells (**A**) or non-labeled 1.4E7 human pancreatic beta cells (**B**, **C**) were embedded in the matrix. Z-stacks with step-size of 0.82 µm for 52 slices (**A**) or 0.418 µm for 82 slices (**B**, **C**) were obtained using LSSM

and fluorescence modality concurrently at 37ºC every 30 sec for 35.5 min (**A**) or every 20 sec for 10 min (**B**, **C**). (**D**) Expansion of channels by migrating T cells. Primary human $CD4^+$ T cells were loaded with CFSE and were embedded in the collagen matrices (Rat tail collagen, 2 mg/ml). Z-stacks with step-size of 1.5 µm for 70 slices were obtained using LSSM and fluorescence modality concurrently at 37ºC every 1 min for 1 hour. (**E**, **F**) Cell-induced displacement of collagen fibers. Non-labeled SK-MEL-5 cells were embedded in rat tail collagen (2 mg/ml). Z-stacks with step-size of 1 µm for 295 slices were obtained using LSSM modality at 37ºC every 1 min for 2 hours. Scale bars are 20 µm. Representative events from three independent experiments are shown.

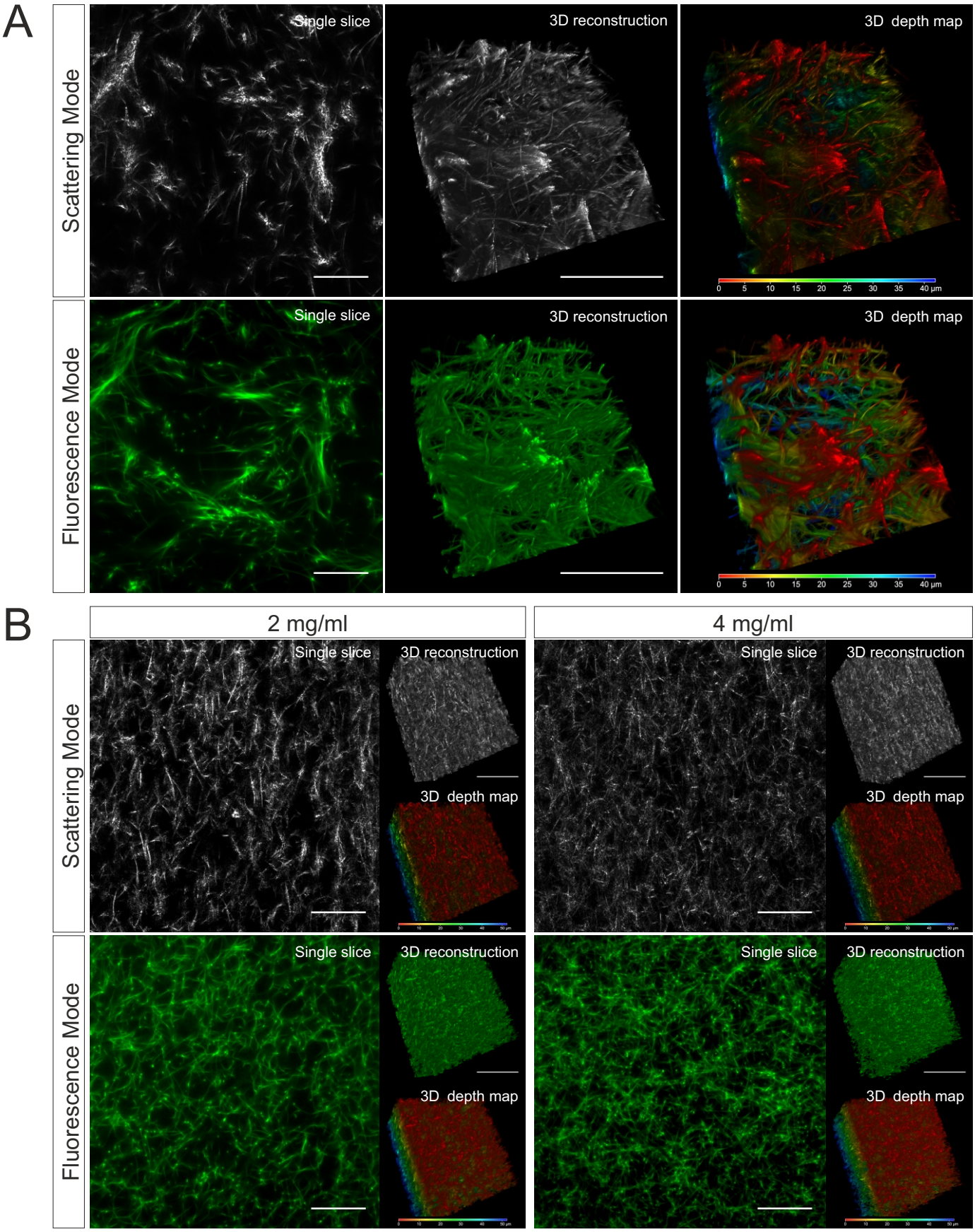
A
Scattering Mode
Fluorescence Mode
Single slice
3D reconstruction
3D depth map
0 5 10 15 20 25 30 35 40 µm
B
2 mg/ml
4 mg/ml
Scattering Mode
Fluorescence Mode
Single slice
3D reconstruction
3D depth map
C
Scattering
Fluorescence
Single slice
3D reconstruction
3D depth map

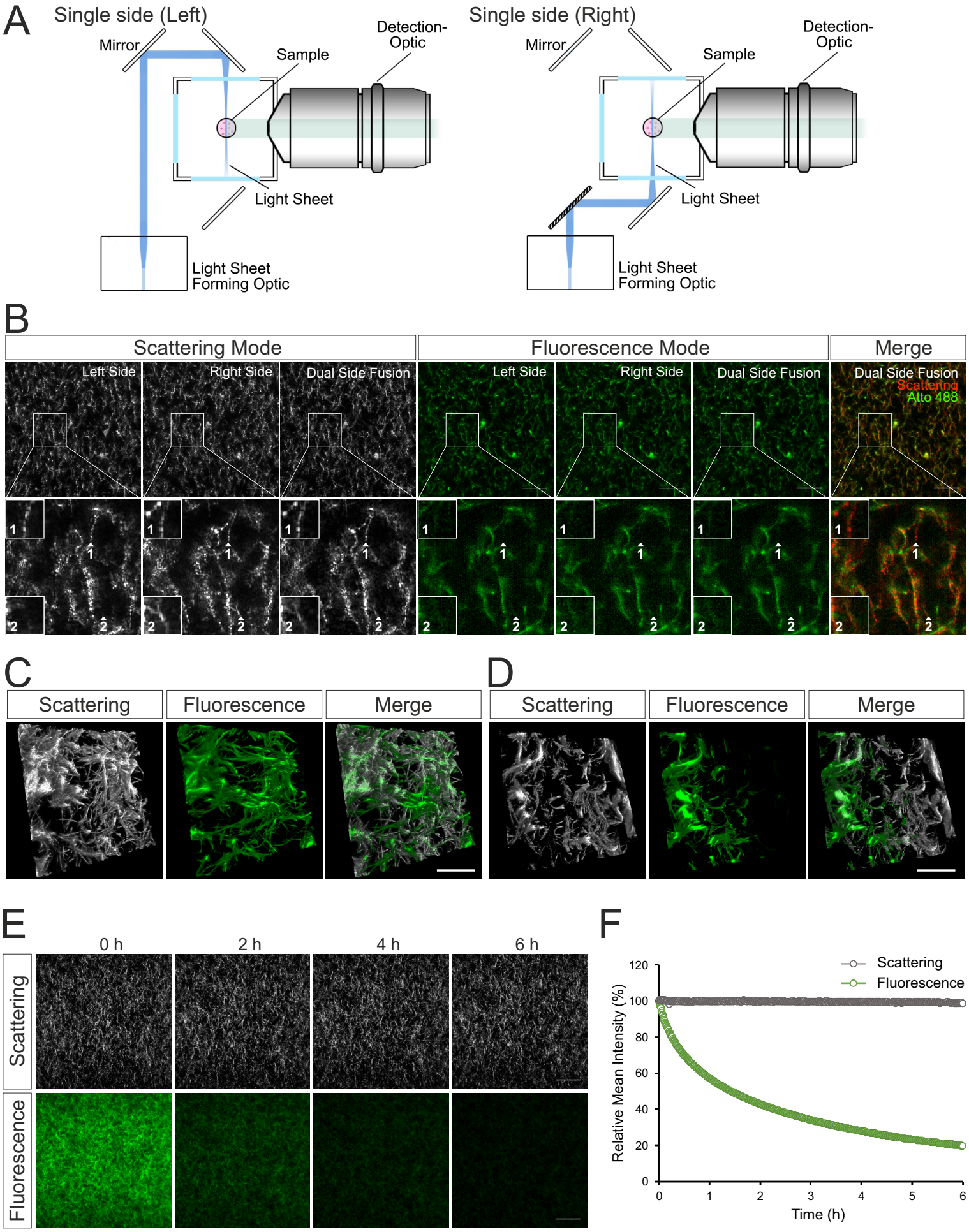
A
Single side (Left)
Mirror
Sample
Detection-Optic
Light Sheet
Light Sheet Forming Optic
Single side (Right)
Mirror
Sample
Detection-Optic
Light Sheet
Light Sheet Forming Optic
B
Scattering Mode
Fluorescence Mode
Merge
Left Side
Right Side
Dual Side Fusion
Left Side
Right Side
Dual Side Fusion
Dual Side Fusion
Scattering
Atto 488
C
Scattering
Fluorescence
Merge
D
Scattering
Fluorescence
Merge
E
0 h
2 h
4 h
6 h
Scattering
Fluorescence
F
Scattering
Fluorescence
Relative Mean Intensity (%)
Time (h)
0
20
40
60
80
100
120
0
1
2
3
4
5
6

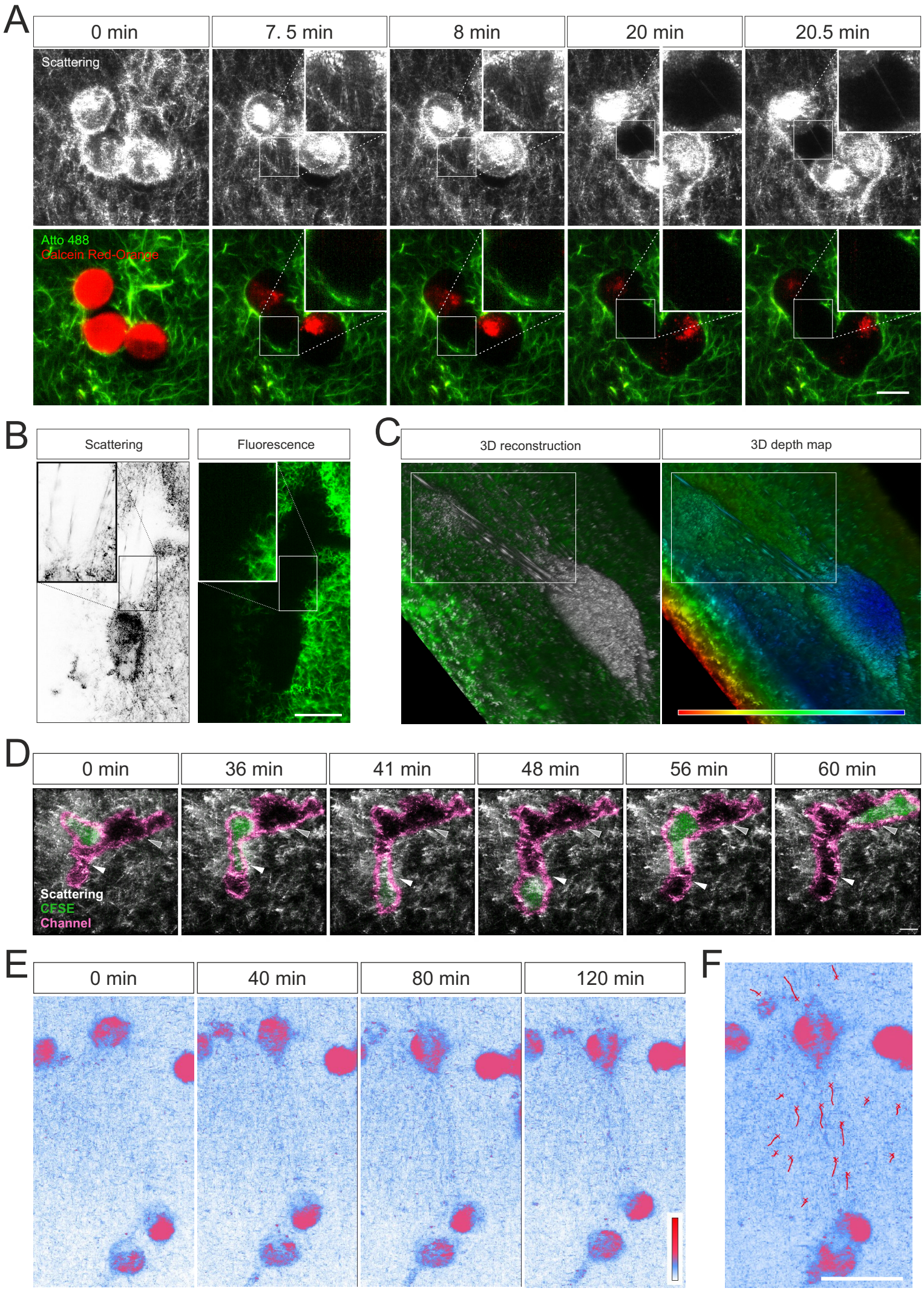
A
0 min
7. 5 min
8 min
20 min
20.5 min
Scattering
Atto 488
Calcein Red-Orange
B
Scattering
Fluorescence
C
3D reconstruction
3D depth map
D
0 min
36 min
41 min
48 min
56 min
60 min
Scattering
CFSE
Channel
E
0 min
40 min
80 min
120 min
F

Supplementary Information

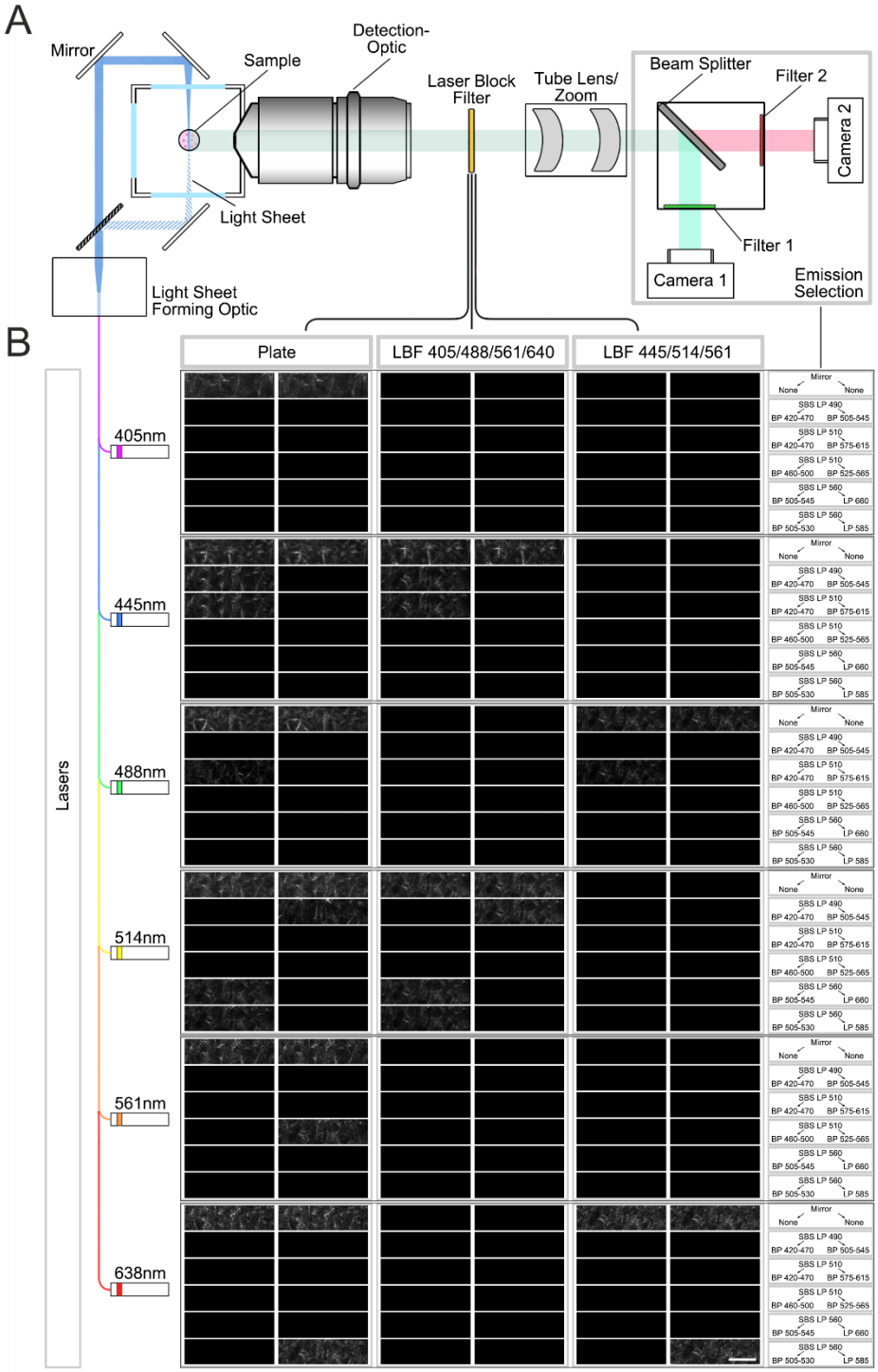

Supplementary Figure. 1 LSRM is available on Zeiss Lightsheet.Z1 and shows great flexibility. (A) A brief illustration of the beam path of Zeiss Lightsheet.Z1. Samples are illuminated by a specially generated light sheet. The emission light and the reflected light is

collected by the objective and then filtered by laser block filter. Emission selection modules consist of beam splitters and filters enable two cameras to collect different wavelengths of emission light simultaneously. (B) A collagen sample (2mg/ml) was tested in all 216 combination of lasers, laser block filters and emission selection modules. In each laser-laser block filter square, the 12 possible emission selection were shown in a sequence as the panel on the right side. In those 35 combination which allowed the same wavelength as the illumination light to reach the camera, the collagen sample was visible. Laser power = 0.2%. Exposure time=149.8 ms. Illumination mode: Single side. Pivot scan: On. Scale bars are 20 μm. Representative images from at least three independent experiments are shown.

Movie legend

Movie1-3. Comparison of reconstructed 3D matrix structures obtained by scattering modality and by fluorescence modality. Rat tail collagen (2 mg/ml) was fluorescently labeled with Atto 488. Z-stacks with step-size of xx μm for xx slices were obtained with LSSM and fluorescence mode subsequentially at 37ºC. Reconstructed 3D matrix structures obtained by fluorescence modality is shown in Movie 1, by LSSM modality in Movie 2. Merged structured from both modalities is shown in Movie 3.

Movie 4. Ultrathin filamentous structures observed with LSSM in SK-MEL-5. Rat tail collagen (2 mg/ml) was fluorescently labeled with Atto 488. Calcein red-orange loaded SK-MEL-5 cells were embedded in the matrix. Z-stacks with step-size of 0.82 μm for 52 slices were obtained using LSSM and fluorescence modality concurrently at 37ºC every 30 sec for 35.5 min. Time points with occurrence of ultrathin filamentous structures is displayed slowly.

Movie 5. Ultrathin filamentous structures observed with LSSM in 1.4E7. Rat tail collagen (2 mg/ml) was fluorescently labeled with Atto 488. Non-labeled 1.4E7 human pancreatic beta cells were embedded in the matrix. Z-stacks with step-size of 0.418 μm for 82 slices were obtained using LSSM and fluorescence modality concurrently at 37ºC every 20 sec for 10 min.

The upper and lower frame highlights the ultrathin filamentous structures and the displacement of matrix networks by the cells, respectively.

Movie 6. Visualization of a migrating T cell in ECM using LSSM. Primary human $CD4^+$ T cells were loaded with CFSE and were embedded in the collagen matrices (Rat tail collagen, 2 mg/ml). Z-stacks with step-size of 1.5 μm for 70 slices were obtained using LSSM (gray) and fluorescence modality (green) concurrently at 37ºC every 1 min for 1 hour.

Movie 7. Visualization of cell-induced displacement of collagen fibers. Non-labeled SK-MEL-5 cells were embedded in rat tail collagen (2 mg/ml). Z-stacks with step-size of 1 μm for 295 slices were obtained using LSSM modality at 37ºC every 1 min for 2 hours. Pseudo color is shown.